WANG, S.-L., FERNANDEZ, C., CAO, W., ZOU, C.-Y., YU, C.-M. and LI, X.-X. 2019. An adaptive working state iterative calculation method of the power battery by using the improved Kalman filtering algorithm and considering the relaxation effect. Journal of power sources [online], 428, pages 67-75. Available from: https://doi.org/10.1016/j.jpowsour.2019.04.089

An adaptive working state iterative calculation method of the power battery by using the improved Kalman filtering algorithm and considering the relaxation effect.

WANG, S.-L., FERNANDEZ, C., CAO, W., ZOU, C.-Y., YU, C.-M. and LI, X.-X.

2019

An adaptive working state iterative calculation method of the power battery by using the improved Kalman filtering algorithm and considering the relaxation effect

Shun-Li Wang[a*], Carlos Fernandez[b], Chun-Mei Yu[a], Chuan-Yun Zou[a], Xiao-Xia Li[a], James Coffie-Ken[a]

[a]*School of Information Engineering, Southwest University of Science and Technology, Mianyang 621010, China;*

[b]*School of Pharmacy and Life Sciences, Robert Gordon University, Aberdeen AB10-7GJ, UK.*

Abstract: The adaptive battery modeling and iterative state calculation in the battery management system is very important for the high-power lithium-ion battery packs, the accuracy of which affects its working performance and safety. The improved Kalman filtering algorithm is developed and applied to realize the iterative calculation process. When it is used to estimate the nonlinear state value of the battery, there is a rounding error in the numerical calculation treatment. As the sigma point is sampled in the unscented transform round from the unscented Kalman filter algorithm, an imaginary number appears resulting in the estimation failure. In order to solve this problem, an improved unscented Kalman filtering method is introduced which combines the decomposition in the calculation process. Meanwhile, an adaptive noise covariance matching method is implied. Experiments show that the proposed method can guarantee the semi-positive and numerical stability of the state covariance, and the estimation accuracy can reach the third-order precision. The estimation error remains 1.60% under the drastic voltage and current change conditions. It can provide a theoretical safety protection basis of the battery management for the lithium-ion battery pack.

Keywords: power battery; relaxation effect; iterative state calculation; unscented Kalman filter; adaptive covariance matching

Corresponding author: Shun-Li Wang. Tel/fax: +86-15884655563. E-mail address: *wangshunli@swust.edu.cn*.

1. Introduction

The Lithium-ion Battery (LiB) has been widely used in the power supply applications, which plays an important role in promoting new energy application technologies. In order to determine the remaining energy prediction, real-time battery management extending its useful life to more accurate monitoring of the battery energy available along with State of Charge (SOC) should be required. In recent years, dozens of schemes have been proposed to improve the SOC estimation accuracy, in which the time integral algorithm to the charge-discharge current is regarded as the most direct method. However, this method has a strong dependence on the initial value and easily causes a cumulative error, which may result in large estimation errors in practical applications [1]. The Open Circuit Voltage (OCV) method uses the measured voltage signals for the periodic correction of the integral SOC estimation process. However, its calculation process value needs to wait for quite a long time before the measurement is made [2], making this strategy not desirable in practice.

The Extended Kalman Filter (EKF) algorithm has become the most common method [3], which linearizes the nonlinear system by ignoring the Taylor-type higher-order terms and computing Jacobi matrices for each calculation cycle. An adaptive EKF-based SOC determination was conducted for LiBs [4] and the SOC inconsistency estimation was investigated by using the mean-difference model along with the EKF algorithm [5]. The EKF-based SOC determination is realized for the LiBs [4] and a temperature compensated model was proposed to realize the SOC estimation of LiBs by using the EKF algorithm for an implantable charger [6]. The robust EKF evaluation was investigated for the SOC estimation [7] and the online internal resistance measurement application was also realized by using the EKF algorithm [8], which is also used for the accurate SOC estimation of LiBs together with a comparative analysis [9]. The SOC estimation of LiB was realized by using the grey EKF algorithm together with a novel OCV modelling method [10]. Meanwhile, an EKF-based SOC estimation algorithm was proposed to realize the safety protection for the Unmanned Aerial Vehicle (UAV) LiB packs.

When the SOC estimation is complicated, the computational cost will be very large and the EKF method is sub-optimal [11]. If the given initial state is inappropriate, the calculation model will be diverging [12]. As a result, the Unscented Kalman Filtering (UKF) algorithm was proposed as a derived SOC estimation algorithm [13], which outperformed the problems of the EKF algorithm consistently in the prediction step term in order to correct the estimation error. The covariance matrix is employed in both of the EKF and UKF algorithms. Due to the existence of the rounding error, the error covariance matrix tends to lose its positive definiteness and symmetry [14], which causes the system to become ill-conditioned and thus make the filter to fail. Many scholars studied the dual Kalman filter and consider it in the SOC estimation [15]. An adaptive method was proposed to realize the SOC estimation of an aeronautical LiB pack based on a reduced particle-UKF algorithm [16]. A wavelet transform-adaptive UKF approach was proposed to realize the SOC estimation of LiB [17] and the model parameters. The joint SOC estimation was investigated by using the H-Infinity and UKF algorithms [18]. The SOC estimation of the battery Energy Storage System (ESS) was constructed by using the adaptive UKF with a statistical estimator noise [19]. An adaptive UKF modeling was conducted for the SOC estimation of LiBs [20]. In addition, a new SOC estimation algorithm was investigated for LiBs by using the fractional UKF algorithm [21]. The battery SOC estimation was also conducted by using the adaptive UKF and Support Vector Machine (SVM) [22]. The real-time UKF-based SOC estimation was also investigated in the RTOS mu COS-II platform [23].

Other methods were also conducted by using the recently new technologies. The SOC estimation was realized for LiBs by using the optimized Levenberg-Marquardt wavelet Neural Network (NN) [24], which was also investigated over a wide temperature range by using the UKF algorithm [25]. The power capability evaluation was conducted for LiBs based on the multi-parameter constraint estimation [26]. The OCV-SOC functional optimization relationship was conducted for the working state monitoring of the aerial LiB pack [27] and an adaptive SOC estimation approach was introduced into the LiB series-connected system [28]. An overview and comparison of online implemented SOC estimation methods were conducted for the LiB [29] and the wavelet transform-adaptive UKF approach was also used [17]. The SOC estimation was realized by using a new dual-polarization-resistance model for Electric Vehicles (EVs) [30] and a novel remaining energy prediction approach was conducted for the large LiB format pack [31].

In this paper, an improved UKF algorithm is introduced into the SOC estimation of the LiB pack to ensure the stability and the semi - positivity of the matrix. Since the covariance noise it sets to be an adaptive value along with the SOC level variation, its accuracy has been greatly heightened. An adaptive identification parameter is introduced into the proposed algorithm in order to match the covariance error matrix adaptively, which updates the real-time noise and improve the SOC estimation accuracy of the LiB packs.

2. Mathematical analysis

2.1. Equivalent circuit modeling

The LiB model is divided into NN model, electrochemical model, Equivalent Circuit Model (ECM) and so on. The NN model requires a large number of experimental data samples, and it is relatively difficult to establish the NN equivalent model. The electrochemical model is based on the battery internal chemical reaction, which estimates the SOC values with high accuracy but requires large amount of calculation, making it only adaptive to the theoretical analysis. The ECMs are the most common application models, including R_{int}, RC, Thevenin, Partnership for a New Generation of Vehicles (PNGV) and Generalized Nested Logit (GNL) models. The Thevenin and PNGV models are most commonly used, but the Thevenin models cannot reflect the steady-state voltage changes in a time period of the LiB pack. GNL is the most complicated model, because its structure is complex. In addition, its parameters are very difficult to be identified, which is conducted by using the experimental results. Furthermore, its accuracy is not improved so much compared with the PNGV model and the Coulomb efficiency of the LiB is practically 1. For this reason, the PNGV model with the

capacitor C_b can be avoided. In this case, the LiB equivalent modelling is that the relaxation effects take much time, therefore, it should be better to use the Thevenin model. This effect can be modelled by using another parallel RC branch as for the polarization effect, instead of using the only series capacitor C_b. As a result, the improved two-order ECM is more suitable to describe the battery status in dynamic environments and can be chosen to realize the state-space characterization of the LiB pack, which is shown in Fig. 1.

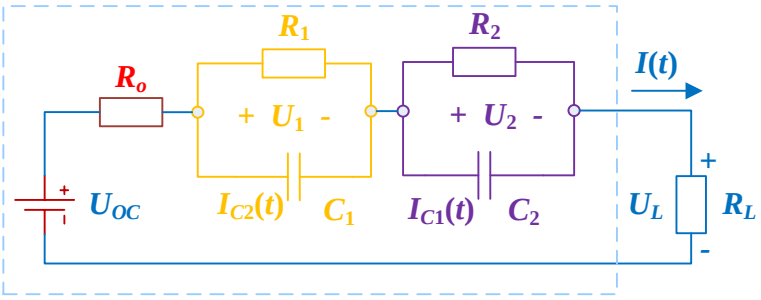

Fig. 1.The two-order equivalent circuit model

In the above ECM circuit, the discharge direction is set as positive and E is the ideal voltage source. The model adds another parallel RC branch based on the Thevenin model, which describes the voltage change along with the accumulation time of the load current. R_o is the ohm resistance of the LiB pack. R_p and C_p are the polarization resistance and capacitance of the battery respectively, which represent the battery charge-discharge polarization characteristics. The battery charge-discharge current is characterized by the parameter of i. U_L is the battery terminal voltage. The time integral to current is regarded as the most direct SOC estimation method, the calculation process of which is shown in Equation 1.

$$\mathrm{SOC(t)} = \mathrm{SOC(t0)} - \int_{t0}^{t} \frac{\eta \mathrm{I}}{3600 C_N} d\tau \tag{1}$$

$SOC(t_0)$ represents the initial SOC value. C_N represents the battery rated capacity which is realized by using the Ampere-hour (Ah) method. The instantaneous current is represented by the parameter of I, in which the discharging direction is set as positive. η represents the Coulomb coefficient. According to the ECM of LiB pack, the parameter SOC is selected as the system state variable uniquely and the battery terminal voltage U_L is set as the observed variable. The state variable dimension is reduced which cuts down the computational complexity greatly, compared with other methods that selected $[SOC\ U_P\ U_b]^T$ as the system stated variables. By taking the discharge direction as positive, the battery state-space equation can be established as shown in Equation 2.

$$\begin{cases} \mathrm{SOC}_k = \mathrm{SOC}_{k-1} - \dfrac{\eta_k \mathrm{T_S}}{\mathrm{Q_N}} \mathrm{I}_{k-1} + w_{k-1} \\ U_{L,k} = \mathrm{U_{oc}}(SOC_k) - \dfrac{T_S}{C_b} \mathrm{I}_{k-1} - \mathrm{R_p}(1 - e^{-\frac{T_S}{C_p R_p}}) \mathrm{I}_{k-1} - R_0 \mathrm{I}_{k-1} + \upsilon_k \end{cases} \quad (2)$$

Wherein, Q_N denotes the battery rated capacity and T_S for the sampling time.

2.2. Parameter identification

The battery internal resistance was measured by conducting the Hybrid Pulse Power Characteristics (HPPC) test, and the principle is described as follows. The current pulses are imposed on the two poles of the LiB, and then the internal parameters can be calculated by detecting the voltage change in each time moment along with the charging-discharging maintenance. In the experiments, the LiBs are produced by AVIC LiB Co. Ltd and taken as the research object, and the experimental test equipment is manufactured by Shenzhen Yakeyuan Technology Co. Ltd. In order to adjust the ambient temperature, the incubator SETH-Z-040L was used for the test. Due to the large variation on the SOC and internal resistance along with the temperature change [32], the change of law of the internal battery resistance and OCV under different temperatures is analyzed. In addition, the temperature correction module is added in the subsequent simulation of the SOC estimation process. The voltage changes in the single one HPPC experiment are shown in Fig. 2.

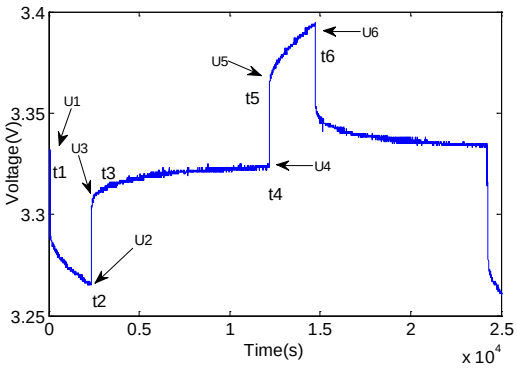

Fig. 2.Battery voltage variation during the HPPC test

According to the Ohm law, the internal resistance of the battery can be calculated by using the formula of $R_o = \Delta U / I$, in which ΔU is the voltage drop of the discharging time moment that can be calculated by $\Delta U = U_1 - U_2$. The relationship can be also obtained similarly when the battery is charged. In the HPPC test, the ohm resistance of the battery disappears instantaneously at the instant of the discharge, leaving only the polarization resistor and capacitor. The polarization resistor can be calculated in accordance with Equation 3.

$$\begin{cases} R_p = \dfrac{U_4 - U_3}{I} \\ \tau = -\dfrac{t_4 - t_3}{\ln\left(1 - \dfrac{U_4 - U_3}{U_1 - U_3}\right)} \end{cases} \tag{3}$$

The energy storage parameter affects the OCV value in the equivalent circuit model, which is obtained by initializing the SOC value and the relationship as shown in Equation 4.

$$C_{\mathrm{p}} = \frac{\tau}{R_{\mathrm{p}}} = -\frac{t_4 - t_3}{R_{\mathrm{p}} \ln\left(1 - \dfrac{U_4 - U_3}{U_1 - U_3}\right)} \tag{4}$$

Wherein, U_{oc} represents the corresponding OCV value of the battery along with different SOC states. The simplified mathematical expression can be used to obtain the C_b value of different SOC states as shown in Equation 5.

$$\begin{cases} \mathrm{E\_}C_b = \dfrac{1}{2}\mathrm{C_b U^2} = \dfrac{1}{2}\mathrm{C_b}(\mathrm{U^2_{100\%SOC}} - \mathrm{U^2_{0\%SOC}}) \\ \mathrm{E\_}C_b = \mathrm{Q_N} * \mathrm{U_{oc}} \end{cases} \tag{5}$$

Wherein, $U_{100\%SOC}$ is the OCV value when the SOC equals to 100%, which can be realized by the CC-CV charging treatment. Similarly, $U_{0\%SOC}$ is the OCV value when the SOC equals to 0% that can be realized by the CC discharging treatment. A series of HPPC tests can be investigated to calculate the battery internal parameters under different SOC states. Taking the OCV value U_{oc} as an example, the SOC is reduced by 0.05 for every discharging time period and a corresponding U_{oc} can be obtained, with 21 discrete data points. The polynomial least square fitting method is adopted as shown in Fig. 3.

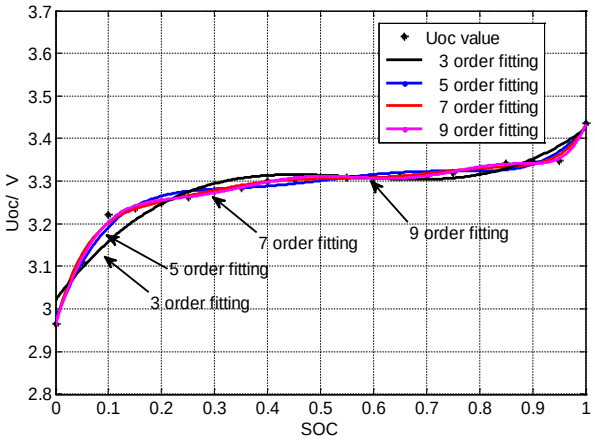

Fig. 3.Fitting effect analysis under different orders

As can be known from Figure 3, it is difficult to guarantee the fitting accuracy by the low-order fitting treatment, and it may lead to over-fitting when using the high-order fitting method. Considering both of the accuracies and computational complexity, the seventh-order fitting method is finally selected. Similarly, the other parameters can be obtained with

different SOC conditions. In order to simplify the model, the polarization resistance and capacitance can be considered as fixed values, which reduces the estimation accuracy undoubtedly.

2.3. Iterative SOC calculation

The battery voltage shows a strong non-linear change in the charge-discharge process. The EKF method expands the nonlinear function by conducting the Taylor expansion and then discards the higher-order terms, which leads to the estimation error increasement. Meanwhile, the derivation of Jacobi matrix increases the computational complexity greatly. Instead of linearizing the nonlinear function, the UKF method approximates probabilistically the density of the nonlinear function. As a result, the estimation accuracy of the UKF is better than EKF, but its value is unstable when the model parameter changes. The improved UKF method solves this problem with the same estimation accuracy, and guarantees the semi-positive and the numerical stability of the covariance matrix. An improved strong tracking UKF algorithm was put forward when studying the satellite attitude determination system [33], which makes better stability, robustness and tracking abrupt state. The discrete state-space equation is shown in Equation 6.

$$\begin{cases} x_k = f(x_{k-1}, u_{k-1}) + \omega_{k-1} \\ y_k = h(x_k, u_k) + \upsilon_k \end{cases} \tag{6}$$

Wherein, f and h represent the nonlinear state equation and observation equation respectively. x_k is the state variable and y_k is the observation variable. u_k is the input variable and ω_k is the system noise, the variance of which is Q_k. v_k is the measurement noise and its variance is R_k. The most computational operation in the iterative UKF-based calculation process is the recalculation of new sigma points in each update step. The difference between improved and traditional UKF algorithms lies in that it uses the improved state variable covariance error instead of the initial values, which transmits the improved covariance directly without investigating the calculation each time. When S is used as the improvement of the covariance matrix P, as $SS^T = P$, P can be guaranteed to be nonnegative as long as $S \neq 0$. Three powerful linear algebra techniques can be used in the improved UKF algorithm including: QR decomposition, Cholesky factor update, and efficient least squares. The improved UKF algorithm mainly includes four parts: initialization, sigma point sampling, time update and status update, which are described in detail as follows.

(1) Initialization

According to the actual situation, the initial value of state variable $\hat{x}_0$ and the initial value of covariance error P_0 can be obtained accordingly. S_0 is the Cholesky factor of covariance, S_0=chol(P_0). The initial values of these parameters can be determined as shown in Equation 7.

$$\begin{cases} \hat{x}_0 = E(x_0) \\ P_0 = E((x_0 - \hat{x}_0)(x_0 - \hat{x}_0)^T) \end{cases} \tag{7}$$

(2) Sigma point sampling

The Unscented Transform (UT) is the core calculation step of the UKF algorithm, and the most critical step of the UT transform contains two parts, namely the sampling strategy selection and the weight coefficient calculation. Herein, the symmetric sampling strategy is adopted to transform *n*-dimensional stated variables into 2**n*+1 *n*-dimensional variables and ensure that the expected and variance of the reference points are unchanged, which can be obtained by Equation 8.

$$x_{k|k}{}^{i} = \begin{cases} \hat{x}_{k|k}, i = 0 \\ \hat{x}_{k|k} + \sqrt{(n+\lambda)} S_k{}^{i}, i = 1...n \\ \hat{x}_{k|k} - \sqrt{(n+\lambda)} S_k{}^{i-n}, i = n+1...2n \end{cases} \tag{8}$$

S_k^i represents the *i*-th column of the Cholesky covariance factor of state variables at the *k* time point, and calculate the mean weight ω_m according to Equation 9.

$$\begin{cases} \omega_{\mathrm{m}}{}^{0} = \dfrac{\lambda}{n+\lambda} \\ \omega_{\mathrm{m}}{}^{i} = \dfrac{1}{2*(n+\lambda)}, \quad i = 1...2n \end{cases} \tag{9}$$

Then, the weight ω_c of the sampling points can be obtained according to Equation 10.

$$\begin{cases} \omega_{\mathrm{c}}{}^{0} = \dfrac{\lambda}{n+\lambda} + 1 - \alpha^2 + \beta \\ \omega_{\mathrm{c}}{}^{i} = \dfrac{1}{2*(n+\lambda)}, \quad i = 1...2n \end{cases} \tag{10}$$

Wherein, *n* is the dimension of the state variables. α is the degree factor that is chosen to determine the closeness degree between the sampling data point and its mean value, which is usually taken as a positive number between 10^{-6} and 1. β means the pre-distribution factor that is optimal for Gaussian distribution, which is set as β = 2. *k* is the auxiliary scale factor, which should satisfy the formula of $k + n \neq 0$. λ is the scaling parameter, which is initialized as $\lambda = \alpha^2 (n + k) - n$. The reasonable adjustment of α and *k* can improve the SOC estimation accuracy of the proposed algorithm.

(3) Time update

According to the state-space equation at *k*-1 time point, the state variables are further predicted by Equation 11.

$$x^{i}_{k|k-1} = f(x^{i}_{k-1|k-1}, u_{k-1}) \tag{11}$$

Then, the overall predicted SOC value can be obtained by Equation 12.

$$\hat{x}_{k|k-1} = \sum_{i=0}^{2n} \omega_m{}^{i} x^{i}_{k|k-1} \tag{12}$$

The QR decomposition of the state variable covariance error is performed according to the one-step prediction of the sampling data points, which is shown in Equation 13.

$$\mathrm{S}_{xk}{}^{-} = qr\{[\sqrt{\omega_c^{1:2n}}(x_{k|k\text{-}1}{}^{1:2n} - \hat{x}_{k|k\text{-}1}), \sqrt{Q_k}]\} \tag{13}$$

Taking the different values of α and k into account may lead $\omega_c{}^0$ to be negative. Therefore, Equation 14 should be used to guarantee the semi-positive of the matrix.

$$\mathrm{S}_{xk} = cholupdate\{S_{xk}{}^{-}, \sqrt{abs(\omega_c{}^0)}(x_{k|k-1}{}^{0} - \hat{x}_{k|k-1}), sign(\omega_c{}^0)\} \tag{14}$$

According to the result of the one-step prediction in Equation 11, one-step prediction of the observed variables are derived from the observation equation as shown in the following equations.

$$\mathrm{y}^{i}_{k|k-1} = h(x^{i}_{k|k-1}, u_k) \tag{15}$$

$$\hat{\mathrm{y}}_{k|k-1} = \sum_{i=0}^{2n} \omega_m{}^{i} y^{i}_{k|k-1} \tag{16}$$

$$\mathrm{S}_{yk}{}^{-} = qr\{[\sqrt{\omega_c^{1:2n}}(\mathrm{y}_{k|k\text{-}1}{}^{1:2n} - \hat{y}_{k|k\text{-}1}), \sqrt{R_k}]\} \tag{17}$$

$$\mathrm{S}_{yk} = cholupdate\{S_{yk}{}^{-}, \sqrt{abs(\omega_c{}^0)}(y_{k|k-1}{}^{0} - \hat{y}_{k|k-1}), sign(\omega_c{}^0)\} \tag{18}$$

(4) Status update

The covariance variance between the state and observed variables can be given by Equation 19, the value of which affects the Kalman gain magnitude directly.

$$P_{xy,k} = \sum_{i=0}^{2n} \omega_c{}^{i}[x^{i}_{k|k-1} - \hat{x}_{k|k-1}][y^{i}_{k|k-1} - \hat{y}_{k|k-1}]^T \tag{19}$$

The Kalman gain is calculated by using the formula as shown in Equation 20.

$$K_k = P_{xy,k}(S_{yk}S_{yk}{}^{T})^{-1} \tag{20}$$

The update of the state variables and their covariance error update can be expressed by Equation 21, in which y_k is the measurement value of the k time point.

$$\begin{cases} \hat{x}_{k|k} = \hat{x}_{k|k-1} + K_k(y_k - \hat{y}_{k|k-1}) \\ S_k = cholupdate(S_{xk}{}^{-}, K_k S_{yk}, -1) \end{cases} \tag{21}$$

2.4. Error correction strategy

In the standard UKF algorithm, the actual noise variance is often difficult to be obtained. In order to simplify the calculation process, the noise covariance is usually regarded as a fixed value for the state and measurement equations. However, the inaccurate noise statistics can reduce the estimation accuracy and even disperse its calculation process [5]. In response to this problem, the adaptive noise covariance matching method is introduced to this interrelate calculation process, which updates and delivers the noise covariance matrix in real time so that it is closer to the real situation. In the system noise update process, the error expression of observational variables at the k time point can be described in Equation 22.

$$e_k = y_k - \hat{y}_{k|k} \tag{22}$$

The variance in the first M time-point errors can be weighted averagely to get the covariance function of H_k, the expression of which can be described in Equation 23.

$$\mathrm{H}_k = \frac{1}{\mathrm{M}} \sum_{i=k-M+1}^{k} \mathrm{e}_k e_k{}^{T} \tag{23}$$

In order to improve the estimation accuracy while reducing the computational complexity as much as possible, the first three updating treatments are conducted in order to realize the calculation process, which is set as $M = 3$. The updating process of the system noise and the observation noise is shown in Equation 24.

$$\begin{cases} Q_k = K_k H_k K_k{}^{T} + H_k \\ R_k = H_k - C_k \mathrm{P}_k C_k{}^{T} \end{cases} \tag{24}$$

Since P_k gradually decreases along with the time passing and finally approaches 0, the P_k part is negligible accordingly.

3. Experimental analysis

3.1. Relevant BMS design

The BMS equipment is designed, which can be used to realize the condition monitoring target of the serially connected single-unit LiB packs of 4, 6, and 8 models on the UAV. It is modularized by the microprocessor and the integrated chip sampling, the size of which is 82*52*15mm. Furthermore, it supports digital communication networking extension, including the Serial Peripheral Interface (SPI) and the Controller Area Network (CAN). It realizes the high-precision real-time detection, in which the accuracy of each cell voltage is 1mV. In addition, it also combines the two-division iterative calculation to realize the SOC estimation, featuring low power consumption, high integration and small size advantages. The relevant BMS device is designed and realized as shown in Fig. 4.

Fig. 4.The relevant BMS device

Through the working condition characteristic analysis of the LiB pack in the UAV, the composite ECM can be constructed. The UKF-based estimation algorithm is improved and the recursive SOC estimation is realized. The equilibrium state influence correcting method is studied for the internal connected battery cells to improve the group SOC calculation accuracy. The proposed algorithm is embedded in the BMS, and the voltage change rate is combined to improve the endurance monitoring accuracy, which provides a basis of the energy controlling adjustment and safety protection of the LiB pack. The experimental platform is shown in Fig. 5.

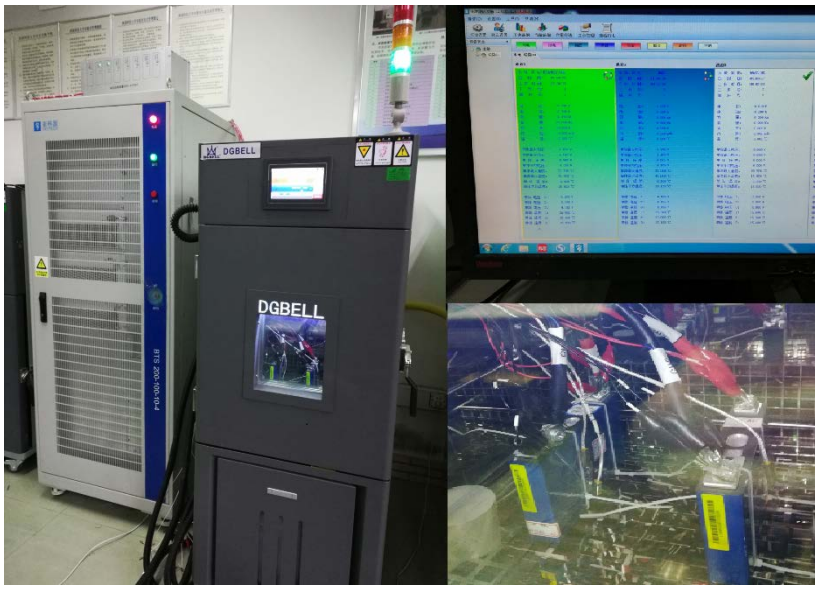

Fig. 5.The experimental platform

The related tests can be investigated by using this experimental platform, the recording data results of which are used to realize the parameter identification of the equivalent model and the SOC estimation results in different working conditions, including the Constant Current (CC) and varying current situations.

3.2.Equivalent modeling verification

Taking the battery parameters into the ECM model, the output voltage waveform measurement can be conducted. The waveform shows that the battery terminal voltage error does not exceed 10mV in this model, the maximum error of which

is not exceeding 0.4%, proving that the accuracy and reliability are suitable for the following research. The comparison curve obtained in the experiments can be described as shown in Fig. 6.

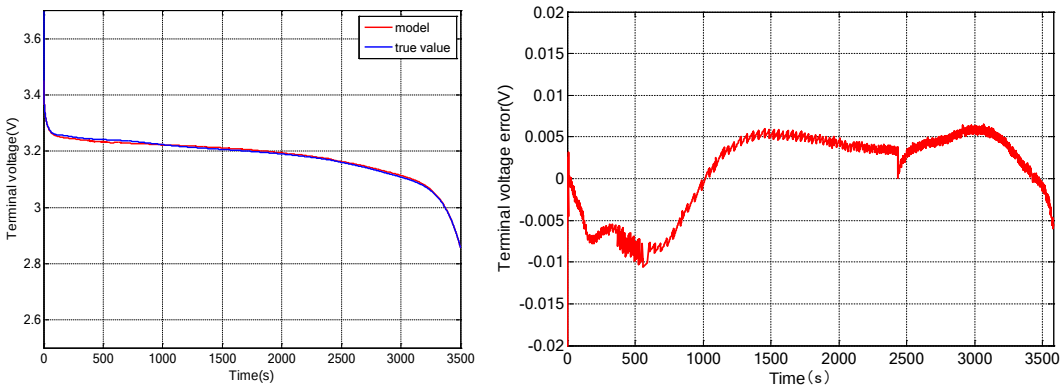

Fig. 6. Terminal voltage and its tracking error

3.3. CC discharging performance

In the CC discharging test, the LiB is fully discharged with a constant current of 1 C_5A. The experimental temperature is 25 ℃, and the model is still applicable to different temperatures. In order to verify the improvement of the proposed algorithm, the traditional and adaptive improved UKF algorithms are used and compared respectively. As can be seen from the local amplification, due to the large discrepancy between the given initial noise covariance and the actual noise covariance at the initial stage of the CC discharge treatment, the traditional UKF algorithm is turbulent and the improved UKF algorithm is relatively better. The improved UKF algorithm converges quickly near the real value and the estimation value almost coincide with the theoretical value, in which the estimated SOC value can follow the theoretical SOC value well until the end of the discharging process. The estimated results of the improved UKF algorithm is far better than the traditional one as shown in Fig. 7.

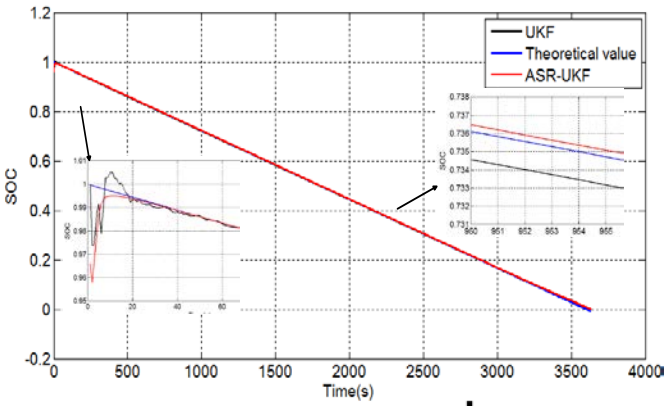

Fig. 7. The comparative SOC estimation in the 1C discharging process

As can be seen from the comparative SOC estimation error curve, the improved algorithm has obvious effect and the error is greatly reduced when it is compared with the error obtained by the UKF algorithm. The maximum error reaches 2.5% due to the internal polarization effect of the battery at the initial and the last discharge time points. The SOC estimation error of the improved UKF algorithm can be also increased to the maximum error which does not exceed 1.4% being the error far below 0.5% during the discharging platform period.

3.4. Different initial value effect

In order to verify the robustness of the improved UKF algorithm to the initial value, the initial SOC value is selected as 0.95, 0.83, 0.53 and 0.1 for the experiments in which the waveform result is shown in Fig. 8.

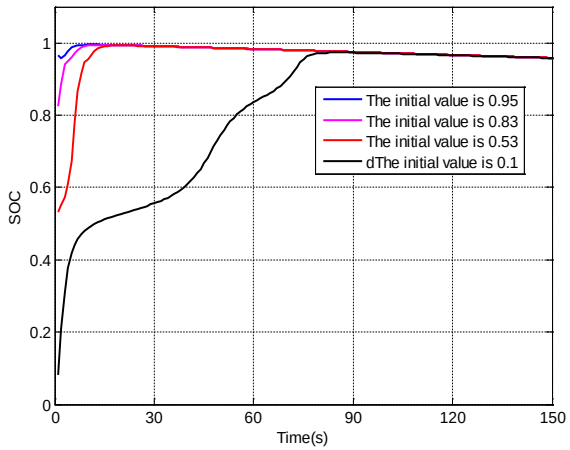

Fig. 8. The SOC estimation effect under different initial values

The constant current discharge of 1 C is performed on the LiB pack under different initial SOC states. The adaptive improved UKF algorithm can converge the initial value of the theoretical vicinity quickly. The closer to the true value, the faster the convergence is. Even if the initial value is set at 0.1 which can be quite different from the actual value, the estimated value can be gradually approximated after a period of correction of about 80s.

3.5. Segmented CC case analysis

In order to analyze the effect of the algorithm on the sudden current change, a varying constant current experiment test is designed. The initial discharging current is 1 C, after a period of time it changes into 0.5 C, 0.3 C, and 0.2 C, the experimental effect of which is shown in Fig. 9.

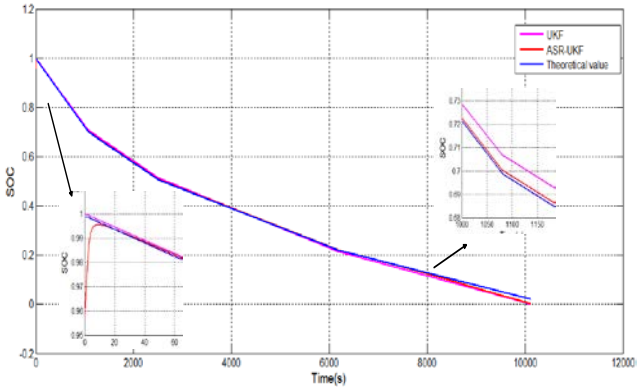

Fig. 9.SOC estimation comparison in the segment constant current

As can be seen from the experimental results, both the improved and the traditional UKF algorithms have good tracking performance when the current is changed. In addition, the estimation accuracy of the improved UKF algorithm is better and the estimation error can be reduced by about 1% at most working conditions compared with the traditional one.

3.6. HPPC test tracking result

In order to verify the effect of improved UKF algorithm under variable current conditions, the strengths and weaknesses for the improved and traditional UKF algorithms are verified by using the HPPC test data. The test procedure is shown as follows. Firstly, a series of pulse tests are carried out with SOC equaling to 1, and then the battery is discharged at a current of 1C to reduce the SOC to 0.95. After one-hour rest, a pulse test can be performed again. The SOC can be reduced by 0.05 in sequence to conduct a pulse test. The voltage waveform is shown in Fig.10.

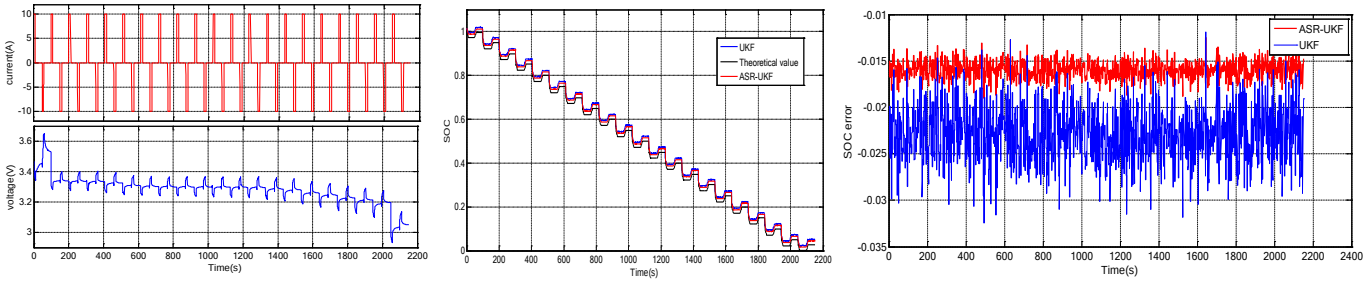

Fig.10 Current-voltage curve and SOC estimation comparison in the HPPC test

The improved and traditional UKF algorithms are applied to the above SOC estimation test, and the estimation results are shown in the waveform error. As can be seen from the experimental results, the improved UKF algorithm can still follow the theoretical SOC value of the drastic voltage and current changing conditions, which reduces the error by about 1.4% compared with the maximum 3.2% error reached by using the traditional UKF algorithm. The maximum error reaches 1.8% in case of drastic voltage and current changes.

4. Conclusion

Due to the rounding error in the numerical calculation, the UKF algorithm has a slow convergence rate for the SOC estimation process of the LiB. Aiming at this problem, QR decomposition is employed into its calculation process, introducing an adaptive improved UKF algorithm. In order to improve the SOC estimation accuracy, a noise adaptive covariance matching module is introduced, in which SOC is used as the state variable. The feasibility of the algorithm is verified under different states: CC discharge, different initial SOC values, piecewise CC and HPPC pulses. Under the constant current discharge condition, the estimated error of improved UKF algorithm is far below 0.5%. Under different initial SOC values, the initial point near the theoretical value can converge quickly. Under the piecewise constant current condition, the estimation error can be reduced by about 1% compared with the traditional one. Under the HPPC test conditions, the maximum error can only be 1.8%. In case of drastic voltage and current changes, the error remains at 1.6%. Experiments show that the problems of negative matrix and unsteady values can be avoided as well as improving the SOC estimation accuracy.

Acknowledgments

This research was supported by National Natural Science Foundation (No. 61801407), RGU.

References

1. Xiong, R., et al., *Critical Review on the Battery State of Charge Estimation Methods for Electric Vehicles.* Ieee Access, 2018. **6**: p. 1832-1843.
2. Shen, Y.Q., *Improved chaos genetic algorithm based state of charge determination for lithium batteries in electric vehicles.* Energy, 2018. **152**: p. 576-585.
3. Cacciato, M., et al., *Real-Time Model-Based Estimation of SOC and SOH for Energy Storage Systems.* Ieee Transactions on Power Electronics, 2017. **32**(1): p. 794-803.
4. Shen, Y.Q., *Adaptive extended Kalman filter based state of charge determination for lithium-ion batteries.* Electrochimica Acta, 2018. **283**: p. 1432-1440.
5. Zheng, Y.J., et al., *State-of-charge inconsistency estimation of lithium-ion battery pack using mean-difference model and extended Kalman filter.* Journal of Power Sources, 2018. **383**: p. 50-58.
6. Lee, K.T., M.J. Dai, and C.C. Chuang, *Temperature-Compensated Model for Lithium-Ion Polymer Batteries With Extended Kalman Filter State-of-Charge Estimation for an Implantable Charger.* Ieee Transactions on Industrial Electronics, 2018. **65**(1): p. 589-596.
7. Huang, C., et al., *Robustness Evaluation of Extended and Unscented Kalman Filter for Battery State of Charge Estimation.* Ieee Access, 2018. **6**: p. 27617-27628.
8. Wang, D., Y. Bao, and J.J. Shi, *Online Lithium-Ion Battery Internal Resistance Measurement Application in State-of-Charge Estimation Using the Extended Kalman Filter.* Energies, 2017. **10**(9).
9. Ramadan, H.S., M. Becherif, and F. Claude, *Extended kalman filter for accurate state of charge estimation of LiBs: a comparative analysis.* International Journal of Hydrogen Energy, 2017. **42**(8): p. 29033-29046.
10. Pan, H.H., et al., *State of charge estimation of lithium-ion batteries using a grey extended Kalman filter and a novel open-circuit voltage model.* Energy, 2017. **138**: p. 764-775.
11. Zheng, Y.J., et al., *Investigating the error sources of the online state of charge estimation methods for lithium-ion batteries in electric vehicles.* Journal of Power Sources, 2018. **377**: p. 161-188.

12. Zheng, L.F., et al., *Incremental capacity analysis and differential voltage analysis based state of charge and capacity estimation for lithium-ion batteries.* Energy, 2018. **150**: p. 759-769.
13. Zhao, W.Z., X.C. Kong, and C.Y. Wang, *Combined estimation of the state of charge of a lithium battery based on a back-propagation- adaptive Kalman filter algorithm.* Proceedings of the Institution of Mechanical Engineers Part D-Journal of Automobile Engineering, 2018. **232**(3): p. 357-366.
14. Zeng, Z.B., et al., *An Online State of Charge Estimation Algorithm for Lithium-Ion Batteries Using an Improved Adaptive Cubature Kalman Filter.* Energies, 2018. **11**(1).
15. Ye, M., et al., *A double-scale and adaptive particle filter-based online parameter and state of charge estimation method for lithium-ion batteries.* Energy, 2018. **144**: p. 789-799.
16. Wang, S.L., et al., *Adaptive State-of-Charge Estimation Method for an Aeronautical Lithium-ion Battery Pack Based on a Reduced Particle-unscented Kalman Filter.* Journal of Power Electronics, 2018. **18**(4): p. 1127-1139.
17. Li, Y.W., C. Wang, and J.F. Gong, *A wavelet transform-adaptive unscented Kalman filter approach for state of charge estimation of LiFePo4 battery.* International Journal of Energy Research, 2018. **42**(2): p. 587-600.
18. Yu, Q.Q., et al., *Lithium-Ion Battery Parameters and State-of-Charge Joint Estimation Based on H-Infinity and Unscented Kalman Filters.* Ieee Transactions on Vehicular Technology, 2017. **66**(10): p. 8693-8701.
19. Peng, S.M., et al., *State of Charge Estimation of Battery Energy Storage Systems Based on Adaptive Unscented Kalman Filter With a Noise Statistics Estimator.* Ieee Access, 2017. **5**: p. 13202-13212.
20. Liu, S.L., N.X. Cui, and C.H. Zhang, *An Adaptive Square Root Unscented Kalman Filter Approach for State of Charge Estimation of Lithium-Ion Batteries.* Energies, 2017. **10**(9).
21. Chen, Y.X., et al., *A New State of Charge Estimation Algorithm for Lithium-Ion Batteries Based on the Fractional Unscented Kalman Filter.* Energies, 2017. **10**(9).
22. Meng, J.H., G.Z. Luo, and F. Gao, *Lithium Polymer Battery State-of-Charge Estimation Based on Adaptive Unscented Kalman Filter and Support Vector Machine.* Ieee Transactions on Power Electronics, 2016. **31**(3): p. 2226-2238.
23. He, H.W., R. Xiong, and J.K. Peng, *Real-time estimation of battery state-of-charge with unscented Kalman filter and RTOS mu COS-II platform.* Applied Energy, 2016. **162**: p. 1410-1418.
24. Xia, B.Z., et al., *State of charge estimation of lithium-ion batteries using optimized Levenberg-Marquardt wavelet neural network.* Energy, 2018. **153**: p. 694-705.
25. Wu, X.G., X.F. Li, and J.Y. Du, *State of Charge Estimation of Lithium-Ion Batteries Over Wide Temperature Range Using Unscented Kalman Filter.* Ieee Access, 2018. **6**: p. 41993-42003.
26. Wang, Y.J., et al., *Power capability evaluation for lithium iron phosphate batteries based on multi-parameter constraints estimation.* Journal of Power Sources, 2018. **374**: p. 12-23.
27. Wang, S.L., et al., *Open circuit voltage and state of charge relationship functional optimization for the working state monitoring of the aerial lithium-ion battery pack.* Journal of Cleaner Production, 2018. **198**: p. 1090-1104.
28. Peng, S.M., et al., *An adaptive state of charge estimation approach for lithium-ion series-connected battery system.* Journal of Power Sources, 2018. **392**: p. 48-59.
29. Meng, J.H., et al., *An Overview and Comparison of Online Implementable SOC Estimation Methods for Lithium-Ion Battery.* Ieee Transactions on Industry Applications, 2018. **54**(2): p. 1583-1591.
30. Zhao, X.W., et al., *State of charge estimation based on a new dual-polarization-resistance model for electric vehicles.* Energy, 2017. **135**: p. 40-52.
31. Zhang, X., et al., *A novel approach of remaining discharge energy prediction for large format lithium-ion battery pack.* Journal of Power Sources, 2017. **343**: p. 216-225.
32. Cheng, Z., et al., *Estimation of State of Charge for Lithium-Ion Battery Based on Finite Difference Extended Kalman Filter.* Journal of Applied Mathematics, 2014.
33. Wang, S.L., et al., *An integrated online adaptive state of charge estimation approach of high-power lithium-ion battery packs.* Transactions of the Institute of Measurement and Control, 2018. **40**(6): p. 1892-1910.